Macromolecules

ARTICLE

pubs.acs.org/Macromolecules

Analytical Rheology of Metallocene-Catalyzed Polyethylenes

Arsia Takeh,[†] Joshua Worch,[‡] and Sachin Shanbhag*,[†]

[†]Department of Scientific Computing, Dirac Science Library, Florida State University, Tallahassee, Florida 32306-4120, United States

[‡]Department of Chemistry, Manchester College, North Manchester, Indiana 46962, United States

ABSTRACT: In this paper, a computational algorithm that seeks to invert the linear viscoelastic spectrum of single-site metallocene-catalyzed polyethylenes is presented. The algorithm uses a general linear rheological model of branched polymers as its underlying engine, and is based on a Bayesian formulation that transforms the inverse problem into a sampling problem. Given experimental rheological data on unknown single-site metallocene-catalyzed polyethylenes, it is able to quantitatively describe the range of values of weight-averaged molecular molecular weight, M_W, and average branching density, b_m, consistent with the data. The algorithm uses a Markov-chain Monte Carlo method to simulate the sampling problem. If, and when, information about the molecular weight is available through supplementary experiments, such as chromatography or light scattering, it can easily be incorporated into the algorithm, as demonstrated.

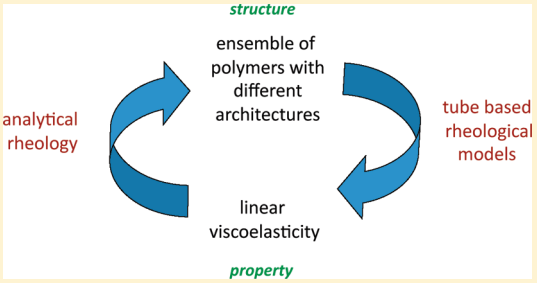

1. INTRODUCTION

When trace amounts of long-chain branching (LCB) is introduced into the backbone of a linear polyethylene molecule, dramatic changes in the linear and nonlinear rheology are observed.[1−5] These well-documented effects include a departure from the "3.4 power law" relating the zero shear viscosity η_0 to the weight-averaged molecular weight M_w, unusually large sensitivity of η_0 to temperature or higher flow activation energies,[6] enhanced shear thinning and strain hardening that lead to improved processability, etc. In polyethylenes, branching in one form or another, has existed since a long time. However, recent developments in single-site metallocene catalyst technology have bestowed us with an extraordinary degree of control on molecular structure, at an industrial-scale. Notwithstanding advances in synthesis, characterization of lightly branched polyethylenes has lagged behind. It has thus become imperative to develop analytical methods that enable us to accurately detect and quantify these trace levels of LCB.[7]

A historically popular approach for diagnosing LCB in synthetic polymers is *g*-ratio analysis, where *g* is the ratio of the size of the branched and linear polymers of the same molecular weight. As Janzen and Colby[7] describe it in their widely cited paper, the "idea is to relate, quantitatively, experimental measurements sensitive to the sizes of polymer molecules in dilute solution, such as light scattering or intrinsic viscosities, to sizes predicted theoretically for structures having specific (regular or random) branching arrangements." These methods rely on theoretical estimates of *g* for different branched structures provided by Zimm-Stockmayer equations.[8,9] Although using only *g*-ratio analysis to detect LCB is fraught with uncertainties,[7] it continues to serve as an important ingredient in more sophisticated multi-detector methods,[2,10] as mentioned later.

A spectroscopic method for directly quantifying the number of long-chain branches is ^{13}C nuclear magnetic resonance (NMR).[11] This method is widely used as a benchmark against which other techniques are compared, despite several practical limitations. For example, NMR is unable to differentiate between short and long branches. It typically cannot distinguish between branches with more than 10 carbon atoms in the side chain, which is far below the "long-chain" threshold of around 100−200 carbon atoms, that are found to affect flow properties so dramatically.[12]

1.1. LCB and Rheology. Both NMR and *g*-ratio analysis are tedious to perform, require expert participation, and are expensive. In addition to these practical difficulties, both these techniques measure fundamentally weak signals. Since the actual number of branch points is often a very small fraction of the total number of backbone carbons, the signal-to-noise ratio becomes a serious issue for ^{13}C NMR.[7,13] Similarly, LCB causes only modest changes in size, which becomes an issue for *g*-ratio analysis. In stark contrast, molecular dynamics are extremely sensitive to molecular structure, and small changes in LCB levels can cause order-of-magnitude changes in rheological properties. In addition, the experimental determination of the linear-viscoelastic spectrum is more straightforward than the other techniques mentioned above. Thus, the use of rheology as an analytical technique ("analytical rheology") to infer details of molecular structure is a compelling idea.[14]

Numerous studies have sought to exploit the sensitivity of rheology to probe LCB in polyolefins. Some determine the departure of melt viscosity η_0 of a branched polymer, from that expected for a linear chain of comparable molecular weight, to quantify LCB via indices. Examples of such methods include the viscosity index of long-chain branching (v.b.i.),[15] Dow rheology index (DRI),[16] long chain branching index (LCBI), etc.[17] A number of more recent studies seek to combine measurements from multiple detectors such as SEC-viscometry, light scattering, melt rheology. etc.[7,17−21]

Received: February 28, 2011
Published: April 07, 2011

Wood-Adams and Dealy[22] used an empirical expression (later linked to molecular theory),[23] to relate differences in the molecular weight distribution (MWD) curves obtained via chromatography and implied by complex viscosity, using Shaw and Tuminello's MWD−viscosity transform for linear polymers,[24] to LCB frequency. Crosby et al.[25] suggested a dilution rheology method, where the concentration-dependent variation of η_0, in conjunction with molecular theory, and rudimentary molecular weight information, was able to quantify the LCB in different families of branched polyethylenes. Similarly, van Ruymbeke et al.[26] developed a criterion to combine molecular weight distribution and linear viscoelastic response, using molecular theory, to detect LCB in sparsely branched polymers with relatively broad molar mass distributions. Robertson et al.[27] measured LCB of polyethylenes with sparse to intermediate levels of LCB and relatively narrow molecular weight distributions, from only linear rheology under certain temperature-frequency windows for the polymers.

While the use of linear viscoelastic measurements for diagnosing LCB is widespread,[2] nonlinear rheological measurements have also been employed. Doerpinghaus and Baird[28] parametrized the pom-pom model, which describes the nonlinear rheology of branched polymers semiquantitatively,[29] to shear and extensional rheology for different levels of LCB. Stadler and Munstedt[30,31] sought to use size-exclusion chromatography with multiangle laser light scattering (SEC−MALLS), and shear rheological measurements to analyze viscosity functions of LCB polyethylenes, by separating the influence of long-chain branching and molecular weight on rheology, which are often convoluted.[32,33] Vittorias et al.[34] employed a combination of Fourier-transform rheology[35] and the pom-pom model[29,36] to determine the topology of branched polymers.

1.2. Bayesian Analytical Rheology. Obtaining structural information from rheological measurements usually requires the inversion of a forward model that is able to predict rheological information from structural measurements. As reviewed above, such forward models may simply be empirical correlations, or based on microscopic theories. The latter have become increasingly sophisticated,[14,37−41] although they are still quite far from being perfect. It is therefore hoped that the extraordinary sensitivity of rheology is able to mask shortcomings in the forward model, to produce sufficiently intelligible structural information. Unlike models for linear chains, hierarchical tube models for branched polymers lack the simple mathematical structure that can be exploited to invert the viscoelastic spectra. Thus, until recently,[42,43] there was no general algorithm which could exploit the flexibility and robustness of these hierarchical models.

As discussed more fully elsewhere,[43] a common method of posing the inverse problem involves seeking the structure that maximizes the agreement between experimental data and model predictions. That is, this approach converts the inverse problem into a well-posed optimization problem. However, despite the intuitive appeal of such an approach, it suffers from an important practical drawback. Optimization assumes uniqueness, since it seeks *the* best or optimal structure, and is incapable of addressing the existence of multiple solutions. Unfortunately, multiple solutions—different structures giving rise to approximately the same rheology—is a common feature.

Shanbhag recently proposed a data analysis method which translated the inverse problem into a sampling problem, using a Bayesian formulation, which was then investigated using a Markov-chain Monte Carlo (MCMC) algorithm.[42,43] By intentionally refraining from seeking "the" optimal solution, this method explored the distribution of structures and compositions consistent with the experimental data, thereby characterizing all possible solutions and associating them with a probability of likelihood. When specifically applied to linears, stars and blends thereof, this method was able to (i) identify the number of components in the unknown mixture, due to the intrinsic Occam's razor in Bayesian analysis,[44−46] (ii) accurately predict the composition of the mixtures, in the absence of degenerate solutions, and (iii) describe multiple solutions, when more than one possible combination of constituents was consistent with the rheology.

Previous work using this methodology was applied on "experimental" data that were synthetically generated using the forward model, and intentionally corrupted with white noise. In this paper, the algorithm is subjected to actual experimental data: linear viscoelasticity (LVE) of metallocene polyethylenes (mPE). What is unique about our computational approach is that instead of assigning a unique value of LCB to the rheological response, this method is able to provide a probability distribution of all possible branched structures consistent with the rheology. As demonstrated in this paper, the method is able to easily incorporate additional information (other than LVE), by the use of so-called prior probabilities.

1.3. Motivation and Scope. The principal aim of this paper is to assess the feasibility of using the recently developed Bayesian inference models for analytical rheology on a technologically relevant problem. mPEs are chosen as the model material because they have the most well-controlled structure among commercially manufactured branched polymers.

We make two key observations regarding the polymerization and linear rheology of mPEs.

- We assume that the polymerization mechanism of these single-site metallocene-catalyzed polyethylenes (see section 2.1) is well established. A particular mPE consists of a mixture of linear and branched polymers. However, due to the assumption of polymerization kinetics, the entire distribution can be characterized by using only two parameters. We provide some evidence for the soundness of this assumption by comparing the GPC curves implied by the polymerization mechanism with the experimental data (Figure 3). While this does not "prove" that the assumption is valid, the consistency of *all* the available experimental and modeled GPC data, indicates that the assumed kinetics are reasonable.
- Based on work by Das et al.[39] on mPE systems, we assume that the forward model offers a good description of the linear rheology. While "reasonable" agreement between forward model and experimental rheology is a prerequisite for the inverse problem, it is critical to realize that the forward model need not be perfect to meaningfully address the inverse problem. While this appears contradictory at first, the reason for the weak requirement is the extreme sensitivity of rheology to structure. If rheology is extremely sensitive to structure, then structure is proportionally insensitive to rheology. To understand this, consider a sensitive mathematical function such as $r = \exp(s)$, where s is a proxy for structure, and r is a proxy for rheology. Small changes in s result in large changes in r. In contrast, the inverse function, $s = \ln(r)$, is far more insensitive to perturbations in r. The point is that the sensitivity that

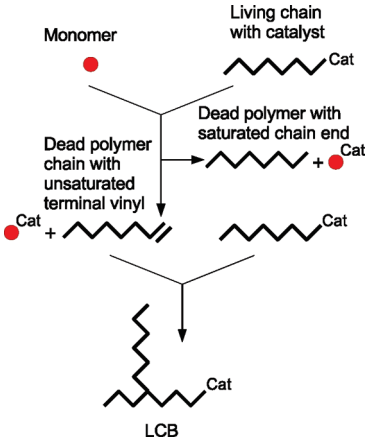

Figure 1. Reaction path for formation of LCB metallocene-polyethylene by Read and McLeish.[48]

makes the forward problem hard, actually makes the inverse problem simpler.

Aided by these two reasonable assumptions, we apply the machinery of Bayesian analysis to assess how successfully we are able to recover the structure of mPE resins, given contemporary models. We pose the problem in two different ways. In the first scenario, we assume that only LVE data is available. In the second scenario, we assume that in addition to LVE, partial structural information in the form of an overall GPC curve is also available.

2. MODEL AND METHOD

In this section, we provide an overview of the polymerization kinetics of single-site mPEs, the available GPC and LVE experimental data, and the Bayesian model.

2.1. Polymerization Kinetics and Molecular Architectures. Soares and Hamielec[47] considered the reaction kinetics of formation of single-site metallocene-catalyzed polyethylenes in a continuous stirred tank reactor. Figure 1 illustrates the four principal steps that lead to the formation of mPE[48]

$$P_{r,i} + M \xrightarrow{k_p} P_{r+1,i}$$

$$P_{r,i} \xrightarrow{k_\beta} D^{=}_{r,i} + P_{1,0}$$

$$P_{r,i} + CTA \xrightarrow{k_{CTA}} D_{r,i} + P_{1,0}$$

$$P_{r,i} + D^{=}_{q,j} \xrightarrow{k_{LCB}} P_{r+q,i+j+1}$$

where P denotes a living polymer, D denotes a dead polymer, M denotes a monomer, and the different "k"s denote the reaction rate constants. The first reaction is propagation, in which a monomer is added to the living chain of length r, containing i LCBs ($P_{r,i}$). In the second, or β-hydride elimination reaction, the catalyst is detached from the living chain to form a dead polymer of the same size. This dead polymer contains an unsaturated terminal vinyl which is subsequently used to form LCB, and $P_{1,0}$ represents a monomer attached to the catalyst. In the third reaction, a living polymer uses chain transfer agent (CTA) to decompose into $P_{1,0}$ and a dead polymer chain with a saturated chain end that plays no role in future reactions. In the final reaction, a dead polymer chain with unsaturated terminal vinyl forms a LCB on a living chain. Soares and Hamielec[47] found that all linear chains, and all segments of branched polymers followed Flory statistics, with a polydispersity index of 2. [The polydispersity index of "molecules" with n branch points is $2(n+1)/(2n+1)$.] Their analytical treatment was in agreement with Monte Carlo simulations which used only two probabilities to characterize chain propagation and branching.

Closely following the kinetics outlined above, Costeux et al.[49] developed an efficient Monte Carlo algorithm to produce the distribution of molecular structures of the resulting mPE polymers. Again, instead of the four rate constants, only two input parameters, viz., the rates of monomer and macromolecular addition relative to the rate of chain termination (defined as the combination of the elimination and CTA steps), were required. This method followed the reaction "in time", and required the storage of all the macromonomers produced from the start.

In contrast, Read and McLeish developed a clever algorithm, which did not follow the reaction in time, and hence overcame this restriction.[48] These different approaches produce identical distributions of molecular architectures; the difference between them is purely algorithmic. Read and McLeish found that in addition to the number average molecular weight of chain segments (Flory distribution), only a single parameter which they called the upstream branching probability b^U, was required to characterize the branching. They introduced ideas of seniority (classification of segments based on their distance from a free end) and priority (number of paths to a free end) to model branched structures, and used distributions of these quantities to predict the rheology.

Thus, two parameters are sufficient to completely characterize the resulting distribution of molecular weight and branching topology. The specific choice of which two parameters to use is practically inconsequential since they are algebraically related. In this paper we use the overall weight-averaged molecular weight M_w, and the average number of branches on a single molecule b_m as the two parameters characterizing the distribution. The latter is closely related to the parameter b^U used in the Read−McLeish algorithm. Given the kinetics, the polydispersity index M_w/M_n, where M_n is the overall number-averaged molecular weight of the sample is given by $M_w/M_n = 2(b_m + 1)$.[49]

Table 1. Molecular Characteristics of Experimental Data[a] Considered in This Paper[2,39]

resin	M_w, g/mol	b_m	λ	PDI
HDB1	77000	0.067	0.026	1.98
HDB2	82000	0.099	0.037	1.93
HDB3	86000	0.116	0.042	1.99
HDB4	96000	0.224	0.080	2.14
HDB5	79000	0.21	0.090	–
HDB6	68000	0.34	0.188	–
HDB7	70000	0.54	0.333	–

[a] M_w is the weight averaged molecular weight, b_m is the average number of branches on a single molecule, λ is the LCB frequency per 1000 backbone C atoms, and PDI is the polydispersity index. The experimental GPC curves were only reported HDB1-HDB4.

2.2. Experimental Data and Preprocessing. Seven sets of metallocene-catalyzed polyethylenes from Wood-Adams et al. are considered in this paper.[2,39] They range between one branch point every 15 molecules (HDB1), to one branch point every other molecule (HDB7). Table 1 shows the molecular characteristics of these resins.

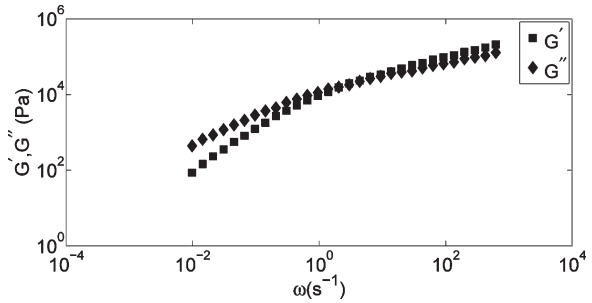

Figure 2. Experimental LVE data for HDB7 (see Table 1), showing storage (squares) and loss (diamonds) moduli. For clarity, only every fifth data point is plotted.

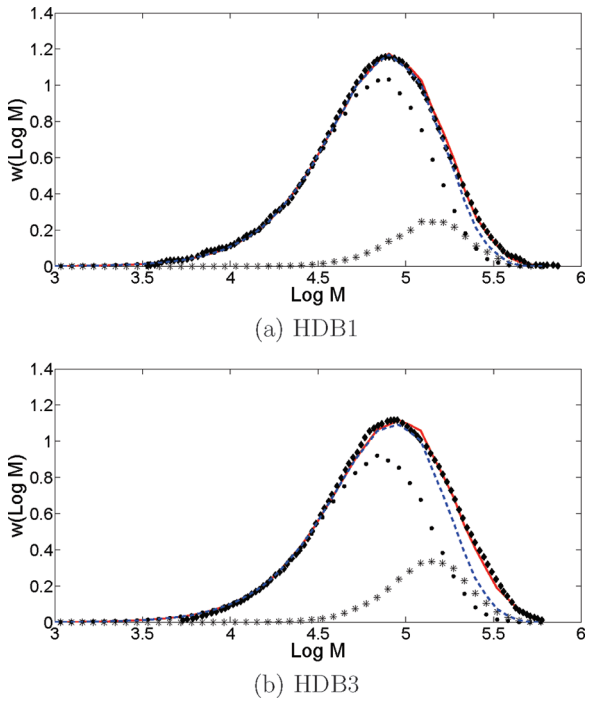

Figure 3. GPC curves for HDB1 and HDB3. Black diamonds and red lines, respectively, are the overall experimental GPC from Wood-Adams et al.[2] and GPC data from BoB. From the simulated samples, we also computed the molecular weight distribution of the linear (filled circles) and star (asterix) fractions. The dotted blue line is the sum of these two contributions, and accounts for most of the mass in a sample.

We digitized the LVE data from published figures. [As a result, the frequencies at which $G'(\omega)$ and $G''(\omega)$ were obtained were usually not identical, which complicates the analysis somewhat. To rectify this, we used cubic splines to interpolate through the raw digitized data, and obtained $G'(\omega)$ and $G''(\omega)$ at equal frequency intervals (on the log−log plot).] Figure 2 depicts such a spectrum for a particular data set (HDB7). We use the symbol **d** as shorthand to denote the experimental dynamic moduli $G'_{exp}(\omega)$ and $G''_{exp}(\omega)$ for a particular data set.

Wood-Adams et al.[2] reported the experimentally measured overall GPC curves only for samples HDB1-HDB4. To test the suitability of the Read−McLeish algorithm in describing the experimental samples, we used the nominal M_w and b_m reported in table 1, to generate the ensemble of branched structures. The overall simulated and experimental GPC curves for all the samples, are in excellent agreement. Figure 3 compares the simulated and experimental GPC for two representative samples, HDB1 and HDB3, for which the experimental data is available. Since we have access to detailed architectural and molecular weight information for the simulated samples, we can probe the contribution of different architectures to the overall GPC curves. In figure 3, we depict some of this information for the two samples. The filled circles and asterixs represent the contributions of the linear and star fractions in a given sample. The dashed blue line is the sum of the linear and star contribution. The proximity of this curve, with the overall GPC reveals that these two architectures (linears and stars) constitute a significant fraction of the overall sample. This is not surprising, since these mPEs are lightly branched. In addition to these GPC curves, the relative fraction of linear, star, comb, and branch-on-branch structures in the simulated data are described in table 2. It should be pointed out that despite the trace quantities of combs and branch-on-branch architectures in the samples considered here, their impact on the LVE is quite substantial.

Table 2. Number and Mass Fractions of Various Structures[a]

resin	n_{lin}	w_{lin}	n_{star}	w_{star}	n_{comb}	w_{comb}	n_{bob}	w_{bob}
HDB1	0.9425	0.8342	0.0504	0.1344	0.0071	0.0314	0.0000	0.0000
HDB2	0.9196	0.7684	0.0674	0.1720	0.0130	0.0596	0.0000	0.0000
HDB3	0.9070	0.7418	0.0747	0.1770	0.0182	0.0803	0.0001	0.0009
HDB4	0.8374	0.5671	0.1161	0.2408	0.0453	0.1825	0.0012	0.0096
HDB5	0.8540	0.6027	0.1053	0.2168	0.0391	0.1656	0.0016	0.0149
HDB6	0.7906	0.4682	0.1351	0.2371	0.0695	0.2576	0.0048	0.0371
HDB7	0.7360	0.3583	0.1462	0.2134	0.1035	0.3235	0.0143	0.1048

[a] n_{lin}, n_{star}, n_{comb}, and n_{bob} are the number fraction of the linear, star, comb and branch-on-branch structures, respectively, in each sample generated by BoB using the Read-McLeish algorithm.[48] Similarly, w_{lin}, w_{star}, w_{comb}, and w_{bob} are the mass fraction of linear, star, comb and branch-on-branch structures, respectively.

Das et al.[39] tested the LVE predictions of the branch-on-branch (BoB) linear rheology model for these data sets, and found that the predicted storage and loss moduli corresponded quite well (except for HDB4) with the experimental LVE. This is a necessary, but not sufficient criteria, for successfully solving the inverse problem.

2.3. Bayesian Formulation. As our forward model we used the branch-on-branch model (BoB) of Das et al.[39] It is a general algorithm based on the tube model and hierarchical relaxation, capable of predicting the linear rheology of arbitrary mixtures of polymers of arbitrary architectures. Its application to mPEs is particularly well-suited, since it includes branch-on-branch architectures, which can dominate the rheology of mPE polymers under certain conditions. For mPE, BoB accepts two-parameter inputs of the type $\bar{\theta} = \{M_w, b_m\}$, where $\bar{\theta}$ is a two-state vector. It produces the corresponding ensemble of molecules, which potentially includes linear, star, H-shaped, and hyper-branched polymers using the efficient algorithm of Read and McLeish.[48] Once the ensemble is generated, it predicts the linear rheology using a time-stepping algorithm to obtain the decay of the time dependent modulus. The corresponding Fourier transforms $G'(\omega)$ and $G''(\omega)$ are denoted by $\mathbf{m}(\bar{\theta})$.

To determine how well a trial value of $\bar{\theta}$ compares with the experimental data $\underline{\mathbf{d}}$, the "error" between the model prediction $\mathbf{m}(\bar{\theta})$ and $\mathbf{d}$, $\varepsilon(\bar{\theta}) = ||\mathbf{d}-\mathbf{m}(\bar{\theta})||$, is defined via a logarithmic

least-squared cost function,

$$\varepsilon(\bar{\theta}) = \frac{1}{2}\sum\left(\log\frac{G'(\omega)}{G'_{\exp}(\omega)}\right)^2 + \frac{1}{2}\sum\left(\log\frac{G''(\omega)}{G''_{\exp}(\omega)}\right)^2 \quad (1)$$

where the summation is over all the discrete values of ω. Logarithms are used to prevent the high-frequency Rouse response from dominating the error.[42] Other reasonable choices are also possible, as discussed elsewhere.[43] A likelihood function $\pi(\mathbf{d}|\bar{\theta})$ which penalizes the error between the experimental and predicted dynamic moduli for a given $\bar{\theta}$, is formulated as $\pi(\mathbf{d}|\bar{\theta}) = e^{-\alpha\varepsilon(\bar{\theta})}$. $1/\alpha$ is analogous to "temperature" in simulated annealing, and controls how severely deviations are penalized. Reducing the value of α admits a large number of plausible structures, and makes distributions broader, while increasing it results in sharper distributions. Therefore, a large value of α may appear desirable. However, this presents two practical difficulties. As $\alpha \to \infty$, which is analogous to a quenching operation, the probability of getting stuck in a local minima becomes large, and results in poor sampling. Second, a large value of α assumes a very high degree of confidence in the underlying forward model, which, in the present case, is not completely warranted. Considering these factors, $\alpha = 10$ is used, throughout this study.

2.3.1. Prior and Posterior Probabilities. As mentioned earlier, in this paper, we consider two scenarios (and perform two types of simulations), depending upon the availability of molecular-weight information. The two scenarios are motivated by considering potential practical applications of analytical rheology of mPEs. It is conceivable that only LVE data (which is easier to measure) on an unknown sample is available, and a quick initial estimate of the M_w and b_m is required. This corresponds to the first scenario, which we label as the "LVE" scenario. However, it is quite routine in industrial practice to run samples through SEC or GPC columns, and often this data is available *in addition to LVE*. This corresponds to the second scenario, which we label as the "LVE+M" scenario, where the experimentally measured M_w, M_w^{exp}, is known. Depending on the scenario, we define a so-called prior probability $\pi(\bar{\theta})$ which summarizes our *a priori* knowledge of the system parameters.

1. *LVE Scenario*: In this case, we assume that the only data available to us is the LVE. That is, we have no information about the experimentally determined weight-averaged molecular weight, M_w^{exp}, or the overall GPC curve. In this case, both the structural parameters used to characterize an unknown mPE sample, M_w and b_M, are unknown. Therefore, we assume a "noninformative" prior probability, $\pi(\bar{\theta}) \sim 1$, which essentially confesses that we have no *a priori* clue about the structure of the mPE sample. We treat this scenario in our simulations as a two-parameter problem, and seek to sample molecular weight and branching content distributions, consistent with the experimental data.
2. *LVE+M Scenario*: It is much easier to measure M_w^{exp} using standard analytical techniques than the branching frequency. If such measurements are available, we can employ a so-called "informative" prior, which in this paper is assumed to be

$$\pi(\bar{\theta}) \sim \delta(M_w - M_w^{\exp}) \quad (2)$$

where δ denotes a Dirac delta function. Note that this choice assumes that M_w^{exp} is measured perfectly. To model experimental uncertainty in the determination of the molecular weight, a normal distribution with a standard deviation which is related to the uncertainty may perhaps be used, instead. Thus, we treat this scenario as a single parameter problem, and seek to sample the distribution of the average number of branches on a single molecule, b_m, consistent with the experimental data.

For either scenario, the posterior probability modifies the corresponding prior probability based on Bayes theorem,

$$\pi(\bar{\theta}|\mathbf{d}) = \frac{\pi(\mathbf{d}|\bar{\theta})\pi(\bar{\theta})}{\sum_{\bar{\theta}}\pi(\mathbf{d}|\bar{\theta})\pi(\bar{\theta})} \quad (3)$$

where $\pi(\mathbf{d}|\bar{\theta})$ is the likelihood function defined earlier, and the denominator is a sum over all possible structures, $\bar{\theta}$. We seek to sample $\pi(\bar{\theta}|\mathbf{d})$ to determine the set of structures, $\bar{\theta}$, consistent with the data $\mathbf{d}$, via eq 3 using a MCMC formulation. The actual mechanics of the MCMC algorithm are described next, and depend on the scenario being considered.

2.3.2. MCMC Algorithm

1. *LVE Scenario*: In this case, the current state $\bar{\theta} = \{M_w, b_m\}$ takes a log-space random step for M_w, and random linear step for b_m to move to the trial state $\bar{\theta}' = \{M'_w, b'_m\}$. The log-space random step for M_w is obtained by setting $M'_w = \beta M_w$, where β is drawn from the distribution $q(\beta) \propto 1/\beta$, for $1/\rho \le \beta \le \rho$. This can be accomplished by drawing a random number x from the uniform distribution $x \in U(0,1)$, and setting $\beta = \rho^{2x-1}$. In this study $\rho = 1.2$, which sets the magnitude of the jump, was used. A random linear step is applied to the b_m by setting $b'_m = b_m + U(-\Delta b_m, \Delta b_m)$ where U denotes a uniform distribution, and $\Delta b_m = 0.1$ in this study, sets the magnitude of the jump. If an unphysical trial move is attempted, which leads to a negative M'_w or b'_m, it is immediately discarded. Otherwise, using detailed balance, the trial $\bar{\theta} \to \bar{\theta}'$ is accepted with the probability,

$$\mathrm{acc}(\bar{\theta} \to \bar{\theta}') = \beta e^{-\alpha[\varepsilon(\bar{\theta}') - \varepsilon(\bar{\theta})]} \quad (4)$$

2. *LVE+M Scenario*: In this scenario, we have the information about the experimentally determined molecular weight M_w^{exp} and using it as a prior probability, via $\pi(\bar{\theta}) \sim \delta(M_w - M_w^{exp}$. Thus, trial moves are confined to a random linear step in b_m, $\bar{\theta} = \{M_w^{exp}, b_m\}$ to $\bar{\theta}' = \{M_w^{exp}, b'_m\}$, where the same process and parameters described above, are used to update $b_m \to b'_m$. For non-negative b'_m, the acceptance probability simplifies to,

$$\mathrm{acc}(\bar{\theta} \to \bar{\theta}') = e^{-\alpha[\varepsilon(\bar{\theta}') - \varepsilon(\bar{\theta})]} \quad (5)$$

The initial state $\bar{\theta}$ was randomly chosen, and the MCMC simulation was carried out as described above. At the end of each MCMC simulation, we obtained a set of configurations and corresponding error values $\{\bar{\theta}, \varepsilon(\bar{\theta})\}$. We only considered states in the top 75th percentile, to discard the burn-in period of the MCMC simulation. The values of simulation parameters $\alpha = 10$, and maximum step sizes in M_w and b_m, via $\rho = 1.2$, and $\Delta b_m = 0.1$, respectively, were chosen heuristically to ensure acceptance probabilities of the order of 0.3.

2.4. Other Assumptions. In the simulations, we assume that the chemistry (polyethylene), polymerization kinetics (single-site metallocene-catalyzed), and the temperature (150 °C) at which the rheological measurement is carried out, are known

precisely. In the *LVE + M* scenario, as mentioned previously, we assume that M_w^{exp} is known precisely. We also assume that the polymerization kinetics and the forward model are reliable. For the forward model, we chose the same parameters as Das et al.,[39] viz. density of 785 kg/m^3, at a temperature of 150 °C, with equilibration time $\tau_e = 1.05 \times 10^{-8}$ s, and entanglement molecular weight M_e = 1120 g/mol. The value of dynamic dilation exponent was set to unity, monomer mass M_0 = 28 g/mol, and number of monomers per entangled segment N_e = 40, in this study.

To describe the mixture of linear and branched polymers in any given mPE sample, we use 50 000 molecules in our MCMC simulations. As pointed out earlier, the algorithm that generates the ensemble of molecules is stochastic. As a result, even for a given M_w and b_m, there is some variation in the exact set of molecules generated. However, if the total number of molecules in the mixture is large, such as the 50 000 molecules considered in this study, the resulting LVE response is quite insensitive.

There is also the perennial question of good sampling of $\bar{\theta}$-space. It should be pointed out that practically it is impossible to be *absolutely certain* that the global minima has been sampled, for nontrivial, and potentially sharp posterior distributions. As described in the next section, we launch several independent MCMC simulations, for a given sample, seeking to avoid getting trapped in local minima.

3. RESULTS AND DISCUSSION

We describe the results for the LVE and the LVE+M scenarios separately.

3.1. LVE Scenario. In the absence of molecular weight information, the Markov chain samples two parameters (M_w and b_m). The local MCMC moves described in 2.3 sample $\bar{\theta}$ using a Boltzmann criteria, where α is analogous to inverse temperature in physical Monte Carlo simulations. The choice of α = 10 makes it possible to jump out of shallow local minima. However, it is still possible to get trapped in relatively deep local minima. To escape trapping, we launched several, independent, moderately long MCMC simulations, with randomly chosen initial states, instead of a single, extremely long run.

We split the simulation into 20 independent runs of 400 MCS. On average, an MCS took about 4−6 min (depending on M_w and b_m) on a single modern processor. Thus, the total computational cost for each resin was about 1 month, on a single processor, with an overall cost of about 7 months for the whole ensemble. However, the sampling process can be easily parallelized. Obviously, each resin can be run on an independent processor. In practice, the 20 independent MCMC chains for each resin were run concurrently on different processors, using the high-throughput computing resources at Florida State University. Thus, the total calendar time required was less than 4 days.

Joint-probability distributions of weight-averaged molecular weight M_w and average number of branches on a single molecule b_m sampled by the MCMC algorithm and postprocessed as described above are presented in figure 4 and figure 5. A gray scale linear color axis is used to represent the "height" of a histogram column, with dark regions corresponding to histogram peaks, and bright regions corresponding to the least frequently sampled values of M_w and b_m. Note that the range of the abscissa and ordinate are chosen to include all the nonzero regions of the sampled joint-probability distributions, and are quite narrow. The range of b_m (ordinate), for instance, only extends approximately ±25% from the axis midpoint, and the corresponding range spanned by M_w is even smaller.

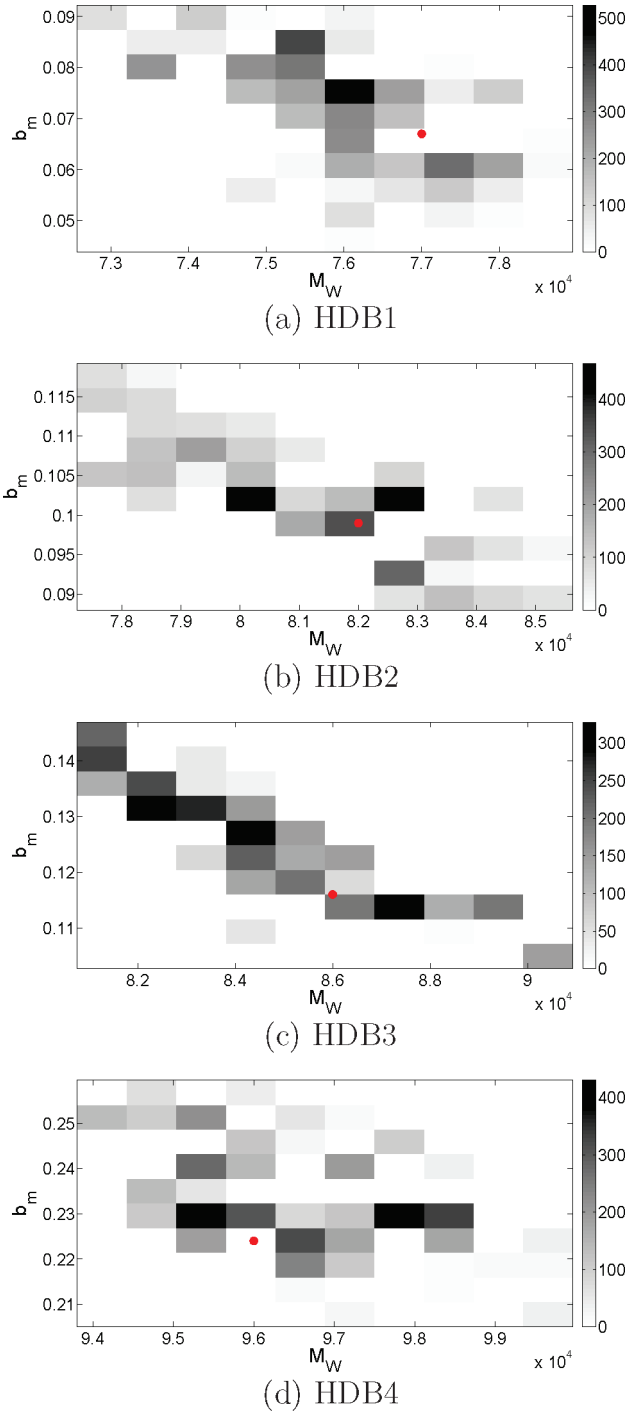

Figure 4. Weight-averaged M_w, and average number of branches on a single molecule, b_m distributions for HDB1, 2, 3, and 4, sampled by the MCMC algorithm. Dark regions correspond to histogram peaks, and the red dot denotes the experimentally determined nominal values of M_w and b_m from table 2.

The results are generally in good agreement with the values experimentally determined by GPC and NMR, indicated by the red dots on the charts. This claim is made in light of fact that the range of the axes are quite narrow, and that there are errors inherent in these standard analytical techniques themselves. Perhaps, the only samples which require additional comment are HDB5 and HDB7. The discrepancy in HDB5 can be traced

dx.doi.org/10.1021/ma2004772 |*Macromolecules* 2011, 44, 3656–3665

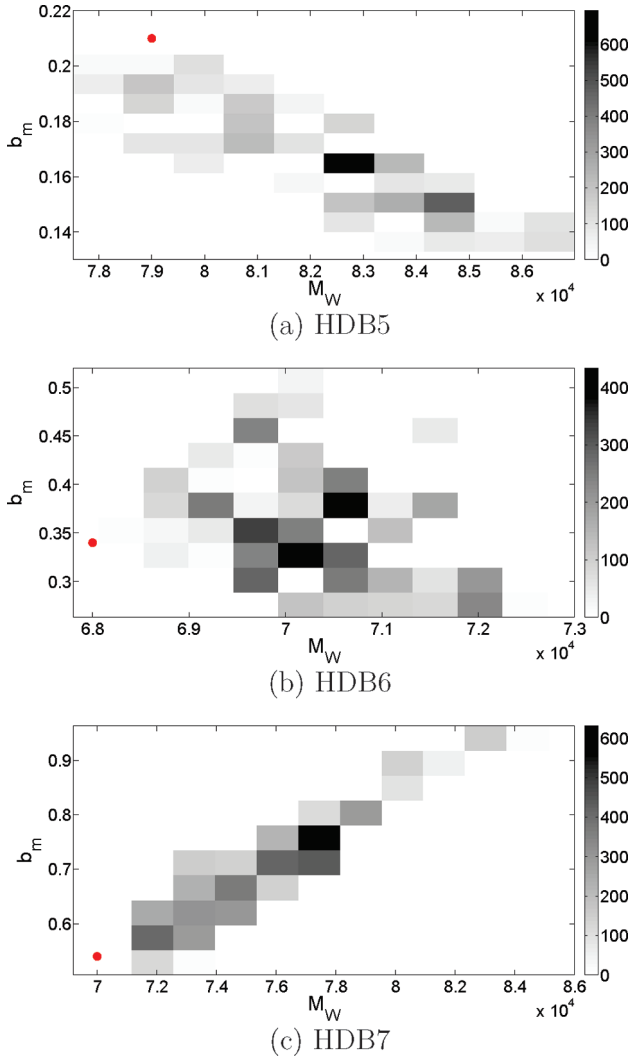

Figure 5. Weight-averaged M_w, and average number of branches on a single molecule, b_m distributions for HDB5-HDB7, sampled by the MCMC algorithm. Dark regions correspond to histogram peaks, and the red dot denotes the experimentally determined nominal values of M_w and b_m from 2.

back to the lack of agreement for this data set found by Das et al.[39]

The lack of agreement for HDB7, for which the predicted values of both M_w and b_m are larger than the experimentally reported numbers, is more subtle. The origin of this discrepancy is immediately obvious, when one considers the original Figure 12 from Das et al.,[39] which is reproduced in Figure 6 for convenience. From Figure 6, it is clear that when one uses the experimentally determined values of M_w and b_m, the predicted relaxation (blue circles) proceeds faster than that observed experimentally (lines). As a crude rule of thumb (with several caveats as discussed in the next section), increasing molecular weight and branching frequency slow down the relaxation, and increase η_0. Hence, the distributions of M_w and b_m in figure 5 lie to the right of the experimental values. Indeed, if one considers only the $\bar{\theta} = (M_w, b_m) = (77100,0.75)$, which corresponds to the configuration with the minimum error sampled in figure 5(c), one obtains the red squares in figure 6, which shows much better agreement with the experimental LVE. The error in this case is $\varepsilon(\bar{\theta} = \{77100,0.75\}) = 0.228$, compared with an error of

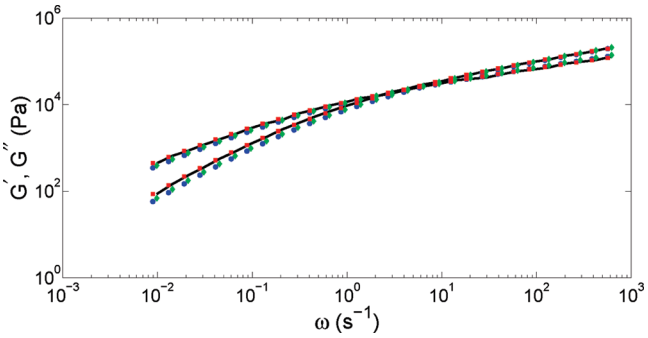

Figure 6. Linear viscoelastic data for HDB7 modeled by BoB using different values of M_w and b_m, and compared with experimental data (lines). Model predictions using the nominal values of M_w and b_m corresponding to HDB7 in 1 are depicted using blue circles. The red squares and green diamonds correspond to the configurations with the least error sampled within the LVE (figure 5c) and LVE+M scenarios (Figure 8c), respectively. Copyright 2006 The Society of Rheology.

$\varepsilon(\bar{\theta} = \{70000,0.54\}) = 2.896$, for the experimentally determined parameters in 1.

3.2. LVE+M Scenario. When M_w^{exp} is available and incorporated into the prior probability, the Markov chains sample only one parameter (b_m). Therefore, the number of MCS required for adequate sampling is considerably smaller. In this study, we considered 7 independent runs (with randomly selected initial configuration) of 300 MCS for each resin. The computational cost for each resin, in this case, was about 9 CPU days with an overall cost of about two CPU months for the whole ensemble. However, the total calendar time required was less than 2 days, since we launched independent runs on separate processors, concurrently.

Results are presented in Figure 7 and figure 8. Since only a single parameter is sampled, we can simplify the graphical representation of the MCMC simulation. Histograms (blue bars) depict the average number of branches on a single molecule, b_m. The experimental values are represented by a thin red line. Once again, the histograms are in good agreement with the experimental data. Marginal distributions of b_m computed from the joint-probability distributions reported for the LVE scenario simulations above, are also presented (empty bars), for comparison. The marginal distribution of b_m, $\pi(b_m)$, is computed by integrating out the effect of M_w from the joint-probability distribution, $\pi(b_m, M_w)$. That is,

$$\pi(b_m) = \int \pi(b_m, M_W)\, dM_W \qquad (6)$$

As expected, the LVE+M scenario results are narrower than the LVE scenario distributions. In general, they are spanned by the LVE scenario results, again as expected, since some of the uncertainty in the b_m distribution is eliminated by specifying M_w.

It is interesting that there is improved agreement for HDB5. The only sample that stands out once again is HDB7. Curiously, there is barely any visible overlap between the distributions obtained in the two scenarios, and they lie on either sides of the experimentally measured b_m. This observation may be understood by revisiting a rule of thumb mentioned previously: generally we expect that increasing M_w and b_m lead to a leftward shift (slower relaxation) of the rheological moduli, or an increase in the zero-shear viscosity η_0. However, HDB7 violates this rule of thumb for b_m, although $d\eta_0/dM_W$ is still positive. As illustrated

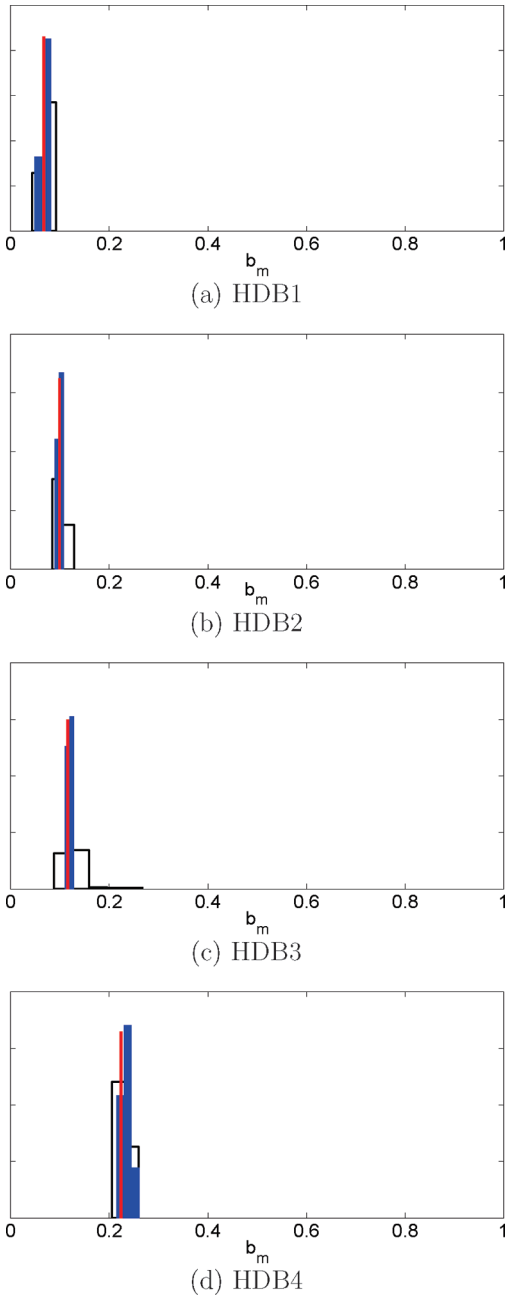

Figure 7. The distribution of b_m for HDB1−HDB4. Experimentally determined values are indicated by the red lines, marginal distribution of b_m from the LVE scenario simulations are indicated by the unfilled bars, and values from the LVE+M scenario are indicated by the blue filled bars.

by Das et al.[39] in Figure 13, parts a and b, of their paper, the η_0 of a mPE with M_w = 70K varies nonmonotonically with b_m. It initially increases, as expected, and then around b_m = 0.4, begins decreasing. At the value of b_m = 0.54 determined by ^{13}C NMR for HDB7, $d\eta_0/db_m$ is *negative*.

The combination of $d\eta_0/dM_w > 0$, and $d\eta_0/db_m < 0$, conspire to cause the observed effect. When we set M_w^{exp} = 70K in the LVE+M scenario, which is lower than the range spanned in figure 5c, we decrease the η_0 below the experimental value. To overcome this faster relaxation, the MCMC simulation seeks to preferentially sample values of b_m that increase the η_0 to match the experimental

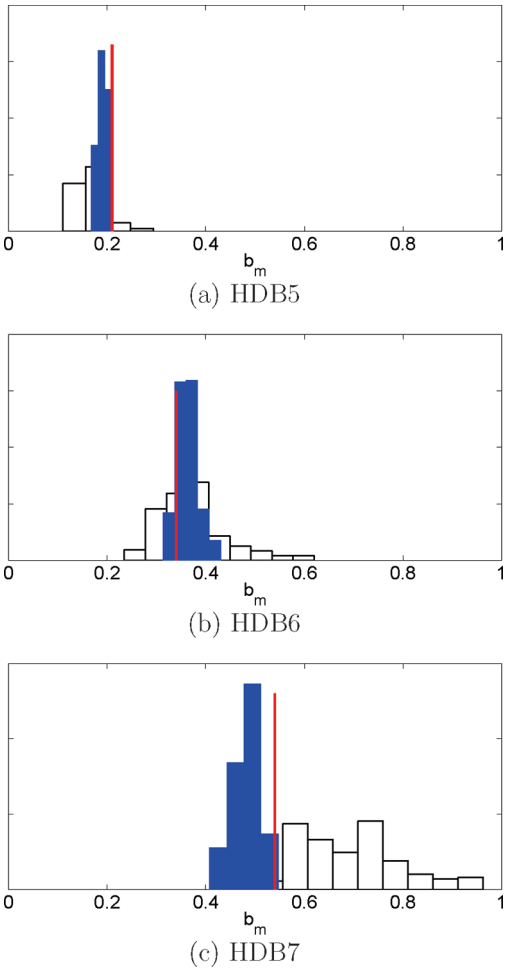

Figure 8. Distribution of b_m for HDB5-HDB7. Experimentally determined values are indicated by the red lines, marginal distribution of b_m from the LVE scenario simulations are indicated by the unfilled bars, and values from the LVE+M scenario are indicated by the blue filled bars.

value. Since $d\eta_0/db_m < 0$, b_m has to be decreased in order to increase η_0, which is precisely what we observe.

It is interesting to note that the least error sampled in the LVE+M scenario with $\varepsilon(\bar{\theta} = \{70000, 0.50\}) = 1.939$ is smaller than the error $\varepsilon(\bar{\theta} = \{70000, 0.54\}) = 2.896$ corresponding to experimental parameters. However, it is larger than $\varepsilon(\bar{\theta} = \{77100, 0.75\}) = 0.228$ corresponding to the least error sampled in the LVE scenario. The run corresponding to the least error configuration in the LVE+M scenario is depicted as green diamonds in Figure 6. The increase in least error sampled as additional information is supplied is not entirely unexpected. As in optimization, providing additional information places constraints on the originally unconstrained solution space, thereby admitting only a subset of original solution space. Since the constrained solution space is a proper subset of the original solution space, the minimum error sampled cannot be lower, and can at best remain unchanged.

3.3. Summarizing Results. Figure 9 summarizes the simulation data ranges for HDB1-HDB7, with subfigures (a) and (b) representing the LVE scenario, and (c) representing the LVE+M scenario. It condenses the information presented in earlier histograms. Clearly, some detailed information reported in the earlier histograms is lost in this process. However, such a

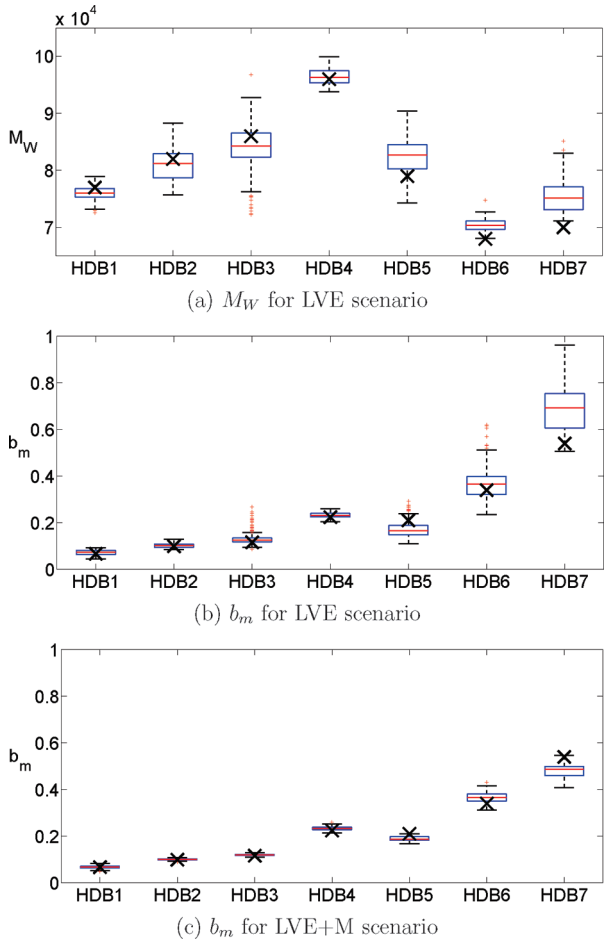

Figure 9. Summary of the data ranges for HDB1-HDB7, with subfigures (a) and (b) representing the LVE scenarios, and (c) representing the LVE+M scenario. The idea here is to reduce the detailed information contained in the probability distributions reported earlier by capturing the essential elements: the median, the variance, existence and number of outliers, and its agreement with the experimentally reported nominal values. It should be pointed out that subfigures (a) and (b) correspond to the marginal distributions of M_w and b_m obtained from the joint probability distributions. The upper and lower bounds (75th and 25th percentile) are captured within the boxes, with the whiskers extending to the maximum and minimum values, not considered outliers (see text for detailed description). Outliers are indicated individually by a "+" sign and the median value for each set is indicated as a solid red line within the box. The "×" sign indicates the experimental M_w or b_m for each set.

birds-eye view of the results allows us to recognize important trends, which are obscured by more detailed representations. The idea here is to reduce the detailed information contained in a histogram, by capturing its essential elements: the median, the variance, existence and number of outliers, and its agreement with the experimentally reported nominal values. It should be pointed out that subfigures (a) and (b) correspond to the marginal distributions of M_w and b_m obtained from the joint probability distributions reported earlier for the LVE scenario. Thus, some information regarding the correlation between M_w and b_m is already lost for these cases.

Particular samples, HDB1 through HDB7, are denoted on the x-axis of the subfigures. In each panel, for a particular sample, a × sign indicates the experimental M_w or b_m (from table 1). The central red line marks the median, and the edges of the blue box represent the values q_1 at the 25th (first quartile), and q_3 at the 75th percentile (third quartile) mark. Thus, the box bounds the central 50% of the sampled configurations around the median, and provides a quick way to visualize the agreement between the experimental and simulated parameters. Note that the median does not necessarily lie at the center of the box, because the histograms are not perfectly symmetrical. The whiskers extend to the most extreme data points not considered outliers, and outliers are plotted individually. Points are considered to be outliers if they are larger than $q_3 + w(q_3 - q_1)$, or smaller than $q_1 - w(q_3 - q_1)$, where $w = 1.5$ was chosen. This choice of $w = 1.5$ corresponds to approximately ±2.76 times the standard deviation and 99.3% coverage, if the data are normally distributed. Thus, a crude way to interpret these graphs is to compare the median and the experimental value, with the bounds of the blue box representing the uncertainty in the median. The range spanned by the whiskers simply provides a higher confidence interval.

4. CONCLUSIONS AND PERSPECTIVE

In this paper, a recently introduced method based on the tube model and Bayesian analysis, was used to implement analytical rheology on lightly branched single-site metallocene catalyzed polyethylenes. The materials are commercially important, and lack a suitable analytical method that can easily describe the level of LCB. Given the linear viscoelastic response of an unknown mPE sample, we were generally able to describe the distribution of M_w and b_m consistent with the data. When additional information on M_w was supplied, it could be easily incorporated into the simulations, via the use of informative prior probabilities, which eased the computational burden, and improved the accuracy of the predictions, simultaneously.

The attractive features of this method are (i) its firm anchor in microscopic theory, (ii) its ability to describe degeneracy, and (iii) its easy incorporation of experimental data in addition to LVE. The use of the microscopic tube model as its underlying engine allows us to leverage the versatility of sophisticated modern formulations that are able to describe arbitrary mixtures of polymers of arbitrary architectures. These models are themselves the subject of intense research, and their improved accuracy has a direct bearing on the proposed method.

The ability to describe a set of structures consistent with the data, instead of a single structure, is a hallmark that perhaps most distinguishes the proposed implementation of analytical rheology. Although degeneracy is not a serious issue for single-site mPEs, it is generally a pervasive feature of inverse problems. Being able to tell whether the available data are sufficient to make a reasonably accurate estimate of the structure is a direct byproduct. Not only can the adequacy of information be assessed, additional experimental information can easily be requested and incorporated to obtain more precise estimates of structure.

The most serious drawback of this algorithm is computational cost. For all the advantages that this technique confers over other methods, it is by far the most computationally demanding. However, the MCMC method lends itself to trivial parallelization, since each trial can run independently, and postprocessed later. With the rising prominence of multicore processors, and the use of graphical processing units (GPU) for computations, this limitation is not as severe as it once was, and will probably become less so.

AUTHOR INFORMATION

Corresponding Author
*Telephone: (850) 644-6548. E-mail: sshanbhag@fsu.edu.

ACKNOWLEDGMENT

This material is based upon work supported by the National Science Foundation under NSF DMR 0953002. We express our gratitude to Dr. Chinmay Das for making the source code to BoB publicly available. We also acknowledge the use of high-throughput computing resources made available by the High-Performance Computing Center at Florida State University.

REFERENCES

(1) Benedikt, G. M.; Goodall, B. L. *Metallocene-catalyzed polymers: Materials, Properties, Processing & Markets*; Plastics Design Library: Norwich, NY, 1998.
(2) Wood-Adams, P. M.; Dealy, J. M.; deGroot, A. W.; Redwine, O. D. *Macromolecules* **2000**, *33*, 7489–7499.
(3) Graessley, W. *Acc. Chem. Res.* **1977**, *10*, 332–339.
(4) Lohse, D. J.; Milner, S. T.; Fetters, L. J.; Xenidou, M.; Hadjichristidis, N.; Mendelson, R. A.; Garcia-Franco, C. A.; Lyon, M. K. *Macromolecules* **2002**, *35*, 3066–3075.
(5) Vega, J.; Aguilar, M.; Peon, J.; Pastor, D.; Martinez-Salazar, J. *e-Polym.* **2002**, *46*, 1–35.
(6) Porter, R.; Knox, J.; Johnson, J. *J. Rheol.* **1968**, *12*, 409.
(7) Janzen, J.; Colby, R. H. *J. Mol. Struct.* **1999**, *486*, 569–584.
(8) Zimm, B. H.; Stockmayer, W. H. *J. Chem. Phys.* **1949**, *17*, 1301–1314.
(9) Billmeyer, F. W., Jr. *J. .Am. Chem. Soc.* **1953**, *75*, 6118–6122.
(10) Yu, Y.; DesLauriers, P.; Rohlfing, D. *Polymer* **2005**, *46*, 5165–5182.
(11) Randall, J. *Polym. Rev.* **1989**, *29*, 201–317.
(12) Liu, W.; Ray, D., III; Rinaldi, P. *Macromolecules* **1999**, *32*, 3817–3819.
(13) Shroff, R. N.; Mavridis, H. *Macromolecules* **2001**, *34*, 7362–7367.
(14) Larson, R. G. *Macromolecules* **2001**, *34*, 4556–4571.
(15) Schreiber, H. P.; Bagley, E. B. *J. Polym. Sci.* **1962**, *58*, 29–48.
(16) Lai, S.; Plumley, T.; Butler, T.; Knight, G.; Kao, C. *SPE Antec Technol.* **1994**, *40*, 1814–1814.
(17) Shroff, R. N.; Mavridis, H. *Macromolecules* **1999**, *32*, 8454–8464.
(18) Wang, W.; Kharchenko, S.; Migler, K.; Zhu, S. *Polymer* **2004**, *45*, 6495–6505.
(19) Vega, J. F.; Fernandez, M.; Santamaria, A.; Munoz-Escalona, A.; Lafuente, P. *Macromol. Chem. Physic.* **1999**, *200*, 2257–2268.
(20) Thimm, W.; Friedrich, C.; Roths, T.; Trinkle, S.; Honerkamp, J. *arXiv: Cond. Mat.* **2000**, *44*, 0009169.
(21) van Ruymbeke, E.; Coppola, S.; Balacca, L.; Righi, S.; Vlassopoulos, D. *J. Rheol.* **2010**, *54*, 507.
(22) Wood-Adams, P. M.; Dealy, J. M. *Macromolecules* **2000**, *33*, 7481–7488.
(23) He, C.; Costeux, S.; Wood-Adams, P. *Polymer* **2004**, *45*, 3747–3754.
(24) Shaw, M. T.; Tuminello, W. H. *Polym. Eng. Sci.* **1994**, *34*, 159–165.
(25) Crosby, B.; Mangnus, M.; de Groot, W.; Daniels, R.; McLeish, T. *J. Rheol.* **2002**, *46*, 401.
(26) van Ruymbeke, E.; Stéphenne, V.; Daoust, D.; Godard, P.; Keunings, R.; Bailly, C. *J. Rheol.* **2005**, *49*, 1503–1520.
(27) Robertson, C. G.; García-Franco, C. A.; Srinivas, S. *J. Polym. Sci., Polym. Phys.* **2004**, *42*, 1671–1684.
(28) Doerpinghaus, P. J.; Baird, D. G. *Macromolecules* **2002**, *35*, 10087–10095.
(29) McLeish, T. C. B.; Larson, R. G. *J. Rheol.* **1998**, *42*, 81–110.
(30) Stadler, F.; Münstedt, H. *Macromol. Mater. Eng.* **2009**, *294*, 25–34.
(31) Stadler, F.; Piel, C.; Kaminsky, W.; Münstedt, H. *Macromol. Symp.* **2006**, *236*, 209–218.
(32) Doerpinghaus, P. J.; Baird, D. G. *J. Rheol.* **2003**, *47*, 717–736.
(33) Laun, H.; Schuch, H. *J. Rheol.* **1989**, *33*, 119.
(34) Vittorias, I.; Parkinson, M.; Klimke, K.; Debbaut, B.; Wilhelm, M. *Rheol. Acta* **2007**, *46*, 321–340.
(35) Fleury, G.; Schlatter, G.; Muller, R. *Rheol. Acta* **2004**, *44*, 174–187.
(36) Inkson, N.; McLeish, T.; Harlen, O.; Groves, D. *J. Rheol.* **1999**, *43*, 873.
(37) Park, S. J.; Shanbhag, S.; Larson, R. G. *Rheol. Acta* **2005**, *44*, 318–330.
(38) van Ruymbeke, E.; Keunings, R.; Bailly, C. *J. Non-Newton. Fluid* **2005**, *128*, 7–22.
(39) Das, C.; Inkson, N. J.; Read, D. J.; Kelmanson, M. A.; McLeish, T. C. B. *J. Rheol.* **2006**, *50*, 207–234.
(40) Larson, R. G.; Zhou, Q.; Shanbhag, S.; Park, S. J. *AIChE J.* **2007**, *53*, 542–548.
(41) Shanbhag, S.; Park, S. J.; Zhou, Q.; Larson, R. G. *Mol. Phys.* **2007**, *105*, 249–260.
(42) Shanbhag, S. *Rheol. Acta* **2010**, *49*, 411–422.
(43) Shanbhag, S. *J. Rheol.* **2011**, *55*, 177–194.
(44) Green, P. J. *Biometrika* **1995**, *82*, 711–732.
(45) MacKay, C. *Bayesian methods for adaptive modelling*; PhD Thesis, California Institute of Technology, 1991.
(46) Murray, I.; Ghahramani, I. *Gatsby Unit Tech. Rep.* **2005**, 1–4.
(47) Soares, J.; Hamielec, A. *Macromol. Theory Simul.* **1996**, *5*, 547–572.
(48) Read, D. J.; McLeish, T. C. B. *Macromolecules* **2001**, *34*, 1928–1945.
(49) Costeux, S.; Wood-Adams, P.; Beigzadeh, D. *Macromolecules* **2002**, *35*, 2514–2528.